Subwavelength hybrid plasmonic nanodisk with high *Q* factor and Purcell factor

2011 J. Opt. 13 075001

(http://iopscience.iop.org/2040-8986/13/7/075001)

J. Opt. **13** (2011) 075001 (5pp) doi:10.1088/2040-8978/13/7/075001

Subwavelength hybrid plasmonic nanodisk with high Q factor and Purcell factor

Yi Song, Jing Wang, Min Yan and Min Qiu

Laboratory of Photonics and Microwave Engineering, School of Information and Communication Technology, Royal Institute of Technology, Electrum 229, 164 40 Kista, Sweden

E-mail: min@kth.se (M Qiu)

Received 23 February 2011, accepted for publication 31 March 2011
Published 28 April 2011
Online at stacks.iop.org/JOpt/13/075001

Abstract
Optical nanodisk resonators based on a hybrid plasmonic waveguiding geometry are investigated theoretically in the wavelength range of 1200–2000 nm with their radii varying from 320 to 1000 nm. Due to the fact that a hybrid plasmonic structure can efficiently confine light in a deep-subwavelength mode volume with a relatively low propagation loss, the nanodisks designed exhibit simultaneously a high Q factor and a high Purcell factor. For a hybrid plasmonic nanodisk with the radius of 1000 nm, a Q factor of 819 and a Purcell factor of 1827 are achieved at the telecommunication wavelength of 1558 nm.

Keywords: hybrid plasmonic nanodisk, Q factor, mode volume, Purcell factor

(Some figures in this article are in colour only in the electronic version)

1. Introduction

There has been a great amount of interest in the research of optical cavities in the last few decades. Such optical cavities are vital for a wide range of applications such as cavity quantum electrodynamics, on-chip light sources (lasers, LEDs, etc), controlled spontaneous emission, optical filters, etc [1]. In applications like single photon sources [2], high-speed modulated lasers [3], threshold-less lasing [4], and investigations of light–matter interactions [5], a cavity with a high quality factor Q and a small volume V, hence a high ratio between the two (recognized as Purcell factor F_P [6]), is desired.

Difficulty arises naturally in maintaining a high Q factor of a cavity when its mode volume is getting smaller. Previous attempts at achieving high-Q and small-volume cavities include photonic crystal cavities [7–9], dielectric nanowire cavities [10–13], dielectric ring or disk cavities [14–20], metal–dielectric cavities [21–24], etc. Although these designs can achieve extremely high Q factors, their mode volumes are limited by the diffraction limit. Therefore achieving a high F_P with these designs is still out of reach. Recently, more and more attention has been paid to plasmonic cavities. Plasmonic devices are based on the surface plasmon polariton effect, which is capable of confining an electromagnetic field at a deep-subwavelength scale. Correspondingly a plasmonic cavity can efficiently reduce the mode volume to an ultrasmall value. However, the existence of Ohmic loss in metals inevitably impinges on the achievable Q factors. The remaining challenge is therefore to reduce the adverse effect of the Ohmic loss inherent to metals deployed in plasmonic light-confining systems.

In this paper, we theoretically study nanodisk cavities based on hybrid plasmonic (HP) structures [25, 26]. With an enhancement of the electromagnetic field inside the low-index layer between a metallic layer and a high-index layer, HP structures can realize a good confinement and relatively low propagation loss simultaneously. Notice that several plasmonic cavities have already been reported [5, 27–30]. However, none of them achieves simultaneously a relatively high Q and a high Purcell factor: for the metal–insulator–metal nanodisk in [27], a small mode volume of $0.000\,33\lambda_0^3$ is achieved experimentally with a high $F_P = 900$ but a low $Q = 16$; for the plasmonic whispering-gallery microcavity in [28], a high Q factor of 1376 ± 65 is reported but unfortunately with a huge mode volume (with radius of $\sim$15 μm); the plasmonic cavity based on a semiconductor nanodisk inside a silver nanopan [29] has a modest mode volume of $0.56(\lambda_0/2n)^3$ with a relatively low $Q = \sim$200; and, more recently, the plasmonic cavity in [5] has a $Q = 100$ and a small $F_P = 18$. In this work, by using an HP

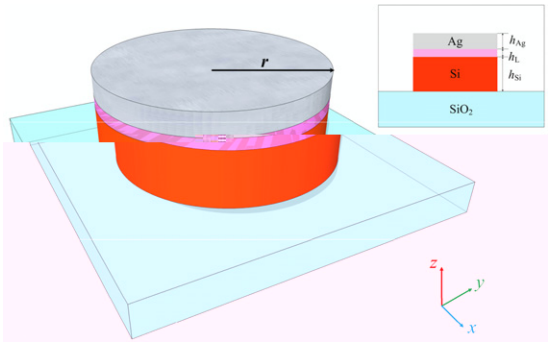

Figure 1. Schematic diagram of the HP nanodisk. The inset shows the cross-section of the HP nanodisk: the silicon layer has a height h_{Si}; the low-index layer has a height h_L; and the silver layer has a height h_{Ag}.

nanodisk with a radius of 1000 nm, we achieve a high $Q = 819$ and a high $F_P = 1827$ simultaneously at the wavelength of 1558 nm.

2. HP nanodisk

The proposed HP nanodisk is schematically depicted in figure 1. Such an HP nanodisk can be fabricated by a two-step process: firstly fabricating a standard SOI microdisk (a 250 nm thick silicon nanodisk on the 3 μm thick silica substrate) by electron beam lithography (EBL) and inductively coupled plasmon (ICP) etching; then a low-index layer and a silver layer are defined on the top of the silicon nanodisk by a second time EBL patterning followed by a lift-off process [31]. Here, the low-index layer will work as a gain medium for the laser and can be fabricated by doping the silica layer with quantum dot nanocrystals [32–35].

A three-dimensional finite-difference time-domain (FDTD) method is used to obtain the field patterns, Q factors, mode volumes, and resonant wavelengths of the HP nanodisks. In order for the operating wavelength to be around the telecommunication wavelength of 1550 nm, the permittivities of the SOI are set to be $\varepsilon_i = 11.9$, $\varepsilon_{SiO2} = 2.1$; the permittivity of the low-index layer should be higher than that of silica because of the doping (here we set it to be $\varepsilon_L = 3$ for convenience); and the dispersive permittivity of the silver is calculated according to a Drude model which is fitted with the experimental data [36]. In the simulations, the heights of the low-index layer and the silver layer are set to be $h_L = 50$ nm and $h_{Ag} = 100$ nm, by which a balance between the propagation loss and the mode confinement can be realized [37].

For the proposed HP nanodisks, there are two different types of modes existing: the transverse electric (TE) mode which is a dielectric-like mode with most electromagnetic energy confined inside the silicon layer; and the transverse magnetic (TM) mode which is a plasmonic-like mode with most electromagnetic energy confined inside the low-index layer. In order to achieve a subwavelength mode confinement and therefore to reduce the mode volume, we only discuss the TM scenario. For nanodisks, there are usually three mode numbers applied to classify the resonant modes, corresponding to the vertical, radial, and azimuthal directions [10]. Here only the fundamental modes in vertical and radial directions are discussed since these modes have higher Q factors and smaller mode volumes compared to the other supported modes. Under these conditions, the modes of the proposed HP nanodisks can be classified with only the azimuthal mode numbers m.

In our FDTD simulations, we firstly set a broad-band Gaussian pulse to excite all of the TM resonant modes in the chosen bandwidth and then we re-run the simulation with narrow-band sources around these modes to obtain the field patterns. For an HP nanodisk with a radius $r = 670$ nm, there is a resonant mode at the wavelength $\lambda = 1552$ nm with the azimuthal number $m = 5$, and the profile of the electric field E_z over a x–y plane in the center of the low-index layer is shown in figure 2(a). To further elucidate the mode confinement, the profile of the electric field E_z in the x–z plane is shown in figure 2(b). The electric field is largely concentrated within the low-index layer and near the sidewall so a relatively small mode volume can be expected.

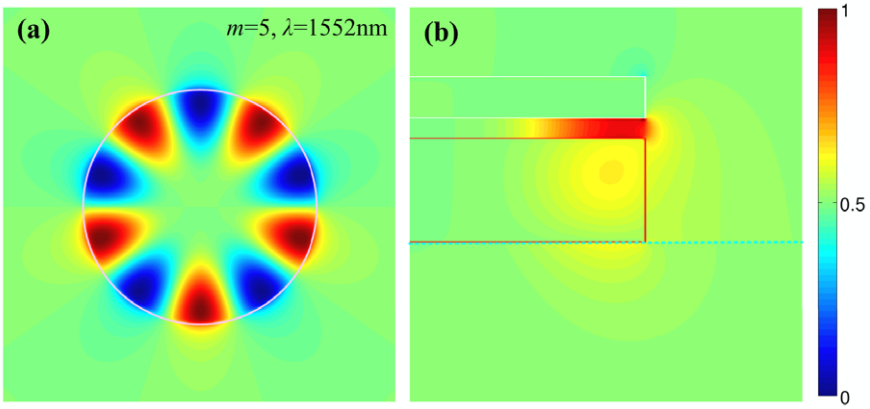

Figure 2. (a) The E_z field distribution in the center of the low-index layer for an HP nanodisk with the radius $r = 670$ nm at $\lambda = 1552$ nm ($m = 5$). The solid line shows the edge of the low-index layer. (b) The E_z field distribution in the x–z plane (half). The solid lines show the silver and silicon layer and the dashed line shows the surface of the silica layer.

3. Simulation results

For a nanodisk cavity, the Q factor is one of the most important parameters to evaluate the properties. To achieve a high Q factor, a common practice is to increase the radius which can effectively decrease the bending-induced radiation loss. However, for an HP nanodisk, a large radius also means a large propagation loss which will also influence the Q factor. At the same time, the increase of the radius will increase the mode volume and influence the Purcell factor.

We have performed FDTD simulations on a number of HP nanodisks whose radii are respectively 320, 440, 560, 670, 780, 890 and 1000 nm. These nanodisk cavities have a resonant mode near the wavelength of 1550 nm, achieved at various azimuthal mode numbers $m = 2$–8. Our FDTD simulation results are summarized in table 1 for a clear comparison of the nanodisk performances. Notice that resonances falling into the telecommunication wavelength regime are highlighted in bold. Here the effective mode volume is calculated as

$$V_{\text{eff}} = \frac{\int \varepsilon(x, y, z)|E(x, y, z)|^2 \, \mathrm{d}x \, \mathrm{d}y \, \mathrm{d}z}{\max\{\varepsilon(x, y, z)|E(x, y, z)|^2\}} \tag{1}$$

and the Purcell factor is calculated as

$$F_{\text{P}} = \frac{3}{4\pi^2}\left(\frac{\lambda_0}{n}\right)^3\left(\frac{Q}{V_{\text{eff}}}\right) \tag{2}$$

where λ_0 is the resonant wavelength in free space and n is the refractive index of the gain medium with $n = \sqrt{3}$. From equation (2), one knows that, in order to obtain a high Purcell factor, it is better to use the resonant mode with a high Q factor and small mode volume.

All the proposed modes supported by these HP nanodisks in the wavelength range of 1200–2000 nm are listed in table 1. As the radius increases, more modes can be supported in an HP nanodisk. In the case of the HP nanodisk with $r = 1000$ nm, six modes are supported in the wavelength range of interest, whereas the nanodisk with $r = 320$ nm has only one mode. For an HP nanodisk with a certain radius, with the increase of the azimuthal number m, the corresponding Q factor also increases. This is caused by the fact that a larger azimuthal number m always means a smaller resonant wavelength, for which both the radiation loss and the propagation loss is smaller. At the same time, as the azimuthal number increases, the mode volume also increases. The variation of the Purcell factor F_{P}, on the other hand, is no longer monotonic, since the Purcell factor depends on both the Q factor and the mode volume. As shown by the last column of table 1, for the HP nanodisk with a small radius ($r < 890$ nm) the Purcell factor F_{P} always increases as the azimuthal number m increases, but for the HP nanodisk with a large radius ($r \geqslant 890$ nm), with the increase of the azimuthal number m, the Purcell factor F_{P} increases first and then decreases.

Table 1. Performance of HP nanodisks with different radii.

Radius (nm)	m	Wavelength (nm)	Q	V_{eff} $((\lambda_0/2n)^3)$	F_{P}
320	**2**	**1569**	**21**	**0.036**	**359**
440	**3**	**1555**	**59**	**0.062**	**579**
	4	1273	169	0.145	708
560	3	1908	46	0.049	570
	4	**1562**	**129**	**0.099**	**790**
	5	1335	336	0.173	1181
670	4	1816	106	0.077	836
	5	**1552**	**268**	**0.131**	**1242**
	6	1364	606	0.226	1630
	7	1226	1227	0.388	1923
780	5	1766	205	0.102	1223
	6	**1552**	**439**	**0.169**	**1579**
	7	1393	833	0.272	1861
	8	1268	1400	0.414	2056
890	5	1970	170	0.091	1138
	6	1733	353	0.146	1468
	7	**1554**	**648**	**0.216**	**1824**
	8	1414	1028	0.347	1801
	9	1301	1532	0.491	1898
	10	1208	2123	0.693	1862
1000	6	1911	299	0.124	1460
	7	1714	518	0.190	1659
	8	**1558**	**8194**	**0.273**	**1827**
	9	1434	1153	0.378	1855
	10	1331	1573	0.527	1814
	11	1244	2098	0.775	1645

For telecommunication applications, we are more interested in the resonant modes near 1550 nm, which has served as a guideline for us to choose the radii of these HP nanodisks in the initial design stage. As a comparison, we plot the Q factors, mode volumes and Purcell factors of these modes in figure 3. As the azimuthal number m increases from 2

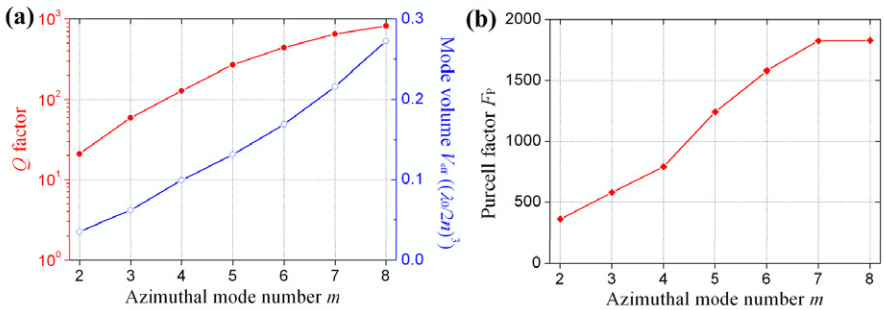

Figure 3. (a) The dependence of the Q factor (solid) and the mode volume (hollow) on the azimuthal mode number m. (b) The dependence of the Purcell factor on the azimuthal mode number m.

Table 2. Performance of HP nanodisks with radius $r = 670$ nm.

h_L (nm)	M	Wavelength (nm)	Q	V_{eff} $((\lambda_0/2n)^3)$	F_P
40	4	1854	116	0.062	1137
	5	**1583**	**283**	**0.105**	**1643**
	6	1389	585	0.172	2066
	7	1244	1047	0.270	2360
50	4	1816	106	0.077	836
	5	**1552**	**268**	**0.131**	**1242**
	6	1364	606	0.226	1630
	7	1226	1227	0.388	1923
60	4	1785	98	0.088	674
	5	**1527**	**254**	**0.174**	**888**
	6	1347	600	0.303	1206
	7	1213	1384	0.501	1678

($r = 320$ nm) to 8 ($r = 1000$ nm), the Q factor increases from 21 to 819 (solid line in figure 3(a)), which is accompanied by an increase of the mode volume from 0.036 to 0.273 $(\lambda_0/2n)^3$ (hollow line in figure 3(a)). To obtain a high Q factor, an HP nanodisk with a large radius (such as $r = 1000$ nm) is a good choice. The dependence of the Purcell factor F_P on the azimuthal number m is plotted in figure 3(b). As the azimuthal number m increases from 2 ($r = 320$ nm) to 7 ($r = 890$ nm), the Purcell factor F_P increases from 359 to 1824 and changes a little to 1827 as m further increases to 8 ($r = 1000$ nm). This means an HP nanodisk with a radius of $r = 890$ nm is large enough to realize a high Purcell factor.

Above we have investigated HP nanodisks with structures having $h_L = 50$ nm. Since the electromagnetic field is strongly concentrated inside the low-index layer, the parameters such as Q factor and mode volume are sensitive to the variation of the height h_L. Here we assess such influence by calculating the modes for HP nanodisks with a fixed radius of 670 nm at various height values for the low-index layer. Table 2 presents the simulation results when the low-index layer height changes from 40 to 60 nm.

When the height h_L varies from 40 to 60 nm, there are always four modes supported in the examined wavelength range of 1200–2000 nm. If one looks at the modes with the same azimuthal mode number, as h_L increases, the mode volume increases apparently due to the larger geometry volume of the low-index layer. The variation of Q factor is more complex. For the modes with $m = 4$ and 5, the Q factor decreases as h_L increases; for the mode with $m = 7$, the opposite trend is noticed; whereas for the mode with $m = 6$, the nanodisk with $h_L = 50$ nm has the highest Q factor. This interesting phenomenon is caused by the trade-off between the radiation loss and the propagation loss: as the height of the low-index layer increases, the propagation loss of the HP nanodisk decreases combined with the increase of the radiation loss caused by the worse mode confinement. The variation of the Purcell factor is simply that F_P monotonically decreases as h_L increases for any m.

4. Conclusions

In conclusion, we have proposed and theoretically studied the performance of a nanodisk resonator based on a hybrid plasmonic structure functioning in the telecommunication wavelength range. Such a plasmonic cavity can achieve a relatively high Q factor and a high Purcell factor simultaneously. For an HP nanodisk with a radius of 1000 nm, a resonant mode with $Q = 819$ can be obtained at the wavelength of 1558 nm and the corresponding Purcell factor is as high as $F_P = 1827$. Our designed HP nanodisk can be predicted to have more application potential in the next generation integrated nanophotonic systems.

Acknowledgments

This work is supported by the Swedish Foundation for Strategic Research (SSF) and the Swedish Research Council (VR).

References

[1] Vahala K J 2003 Optical microcavities *Nature* **424** 839–46
[2] Pelton M, Santori C, Vučković J, Zhang B, Solomon G S, Plant J and Yamamoto Y 2002 Efficient source of single photons: a single quantum dot in a micropost microcavity *Phys. Rev. Lett.* **89** 233602
[3] Altug H, Englund D and Vuckovic J 2006 Ultrafast photonic crystal nanocavity laser *Nat. Phys.* **2** 484–8
[4] Zhang Y, Khan M, Huang Y, Ryou J, Deotare P, Dupuis R and Lončar M 2010 Photonic crystal nanobeam lasers *Appl. Phys. Lett.* **97** 051104
[5] Ma R-M, Oulton R F, Sorger V J, Bartal G and Zhang X 2011 Room-temperature sub-diffraction-limited plasmon laser by total internal reflection *Nat. Mater.* **10** 110
[6] Purcell E M 1946 Spontaneous emission probabilities at radio frequencies *Phys. Rev.* **69** 681
[7] Akahane Y, Asano T, Song B S and Noda S 2003 High-Q photonic nanocavity in a two-dimensional photonic crystal *Nature* **425** 944–7
[8] Song S, Noda S, Asano T and Akahane Y 2005 Ultra-high-Q photonic double-heterostructure nanocavity *Nat. Mater.* **4** 207–10
[9] Zhang Z Y and Qiu M 2004 Small-volume waveguide-section high Q microcavities in 2D photonic crystal slabs *Opt. Express* **12** 3988–95
[10] Johnson J C, Choi H J, Knutsen K P, Schaller R D, Yang P and Saykally R J 2002 Single gallium nitride nanowire lasers *Nat. Mater.* **1** 106–10
[11] Huang M H, Mao S, Feick H, Yan H, Wu Y, Kind H, Weber E, Russo R and Yang P D 2001 Room temperature ultraviolet nanowire nanolasers *Science* **292** 1897–9
[12] Duan X F, Huang Y, Agarwal R and Lieber C M 2003 Single-nanowire electrically driven lasers *Nature* **421** 241–5
[13] Qian F, Li Y, Gradecak S, Park H G, Dong Y, Ding Y, Wang Z L and Lieber C M 2008 Multi-quantum-well nanowire heterostructures for wavelength-controlled lasers *Nat. Mater.* **7** 701–6
[14] McCall S L, Levi A F J, Slusher R E, Pearton S J and Logan R A 1992 Whispering-gallery mode microdisk lasers *Appl. Phys. Lett.* **60** 289–91
[15] Xu Q, Schmidt B, Pradhan S and Lipson M 2005 Micrometre-scale silicon electro-optic modulator *Nature* **435** 325
[16] Shainline J, Elston S, Liu Z, Fernandes G, Zia R and Xu J 2009 Subwavelength silicon microcavities *Opt. Express* **17** 23323–31
[17] Liu Z, Shainline J M, Fernandes G E, Xu J, Chen J and Gmachl C F 2010 Continuous-wave subwavelength microdisk lasers at $\lambda = 1.53$ μm *Opt. Express* **18** 19242–8

[18] Kippenberg T J, Spillane S M, Armani D K and Vahala K J 2003 High-Q ring resonators in thin siliconon-insulator *Appl. Phys. Lett.* **83** 797
[19] Xu Q, Manipatruni S, Schmidt B, Shakya J and Lipson M 2007 12.5 Gbit/s carrier-injection-based silicon micro-ring silicon modulators *Opt. Express* **15** 430–6
[20] Zhang Z, Dainese M, Wosinski L and Qiu M 2008 Resonance-splitting and enhanced notch depth in SOI ring resonators with mutual mode coupling *Opt. Express* **16** 4621–30
[21] Hill M T *et al* 2007 Lasing in metallic-coated nanocavities *Nat. Photon.* **1** 589–94
[22] Manolatou C and Rana F 2008 Subwavelength nanopatch cavities for semiconductor plasmon lasers *IEEE J. Quantum Electron.* **44** 435–47
[23] Nezhad M P, Simic A, Bondarenko O, Slutsky B, Mizrahi A, Feng L, Lomakin V and Fainman Y 2010 Room-temperature subwavelength metallo-dielectric lasers *Nat. Photon.* **4** 395–9
[24] Yu K, Lakhani A and Wu M C 2010 Subwavelength metal-optic semiconductor nanopatch lasers *Opt. Express* **18** 8790–9
[25] Oulton R F, Sorger V J, Genov D A, Pile D F P and Zhang X 2008 A hybrid plasmonic waveguide for subwavelength confinement and long-range propagation *Nat. Photon.* **2** 496–500
[26] Dai D and He S 2009 A silicon-based hybrid plasmonic waveguide with a metal cap for a nano-scale light confinement *Opt. Express* **17** 16646–53
[27] Kuttge M, Garca de Abajo F J and Polman A 2010 Ultrasmall mode volume plasmonic nanodisk resonators *Nano Lett.* **10** 1537–41
[28] Min B, Ostby E, Sorger V, Ulin-Avila E, Yang L, Zhang X and Vahala K 2009 High-Q surface-plasmon-polariton whispering-gallery microcavity *Nature* **457** 455–8
[29] Kwon S H, Kang J H, Seassal C, Kim S K, Regreny P, Lee Y H, Lieber C M and Park H G 2010 Subwavelength plasmonic lasing from a semiconductor nanodisk with silver nanopan cavity *Nano Lett.* **10** 3679–83
[30] Oulton R F, Sorger V J, Zentgraf T, Ma R-M, Gladden C, Dai L, Bartal G and Zhang X 2009 Plasmon lasers at deep subwavelength scale *Nature* **461** 629–32
[31] Wang J, Song Y, Yan M and Qiu M 2010 Efficient coupler between silicon waveguide and hybrid plasmonic waveguide *Proc. SPIE* **7987** 79870B
[32] Wundke K, Pötting S, Auxier J, Schülzgen A, Peyghambarian N and Borrelli N F 2000 PbS quantum-dot-doped glasses for ultrashort-pulse generation *Appl. Phys. Lett.* **76** 10
[33] Malko A V, Mikhailovsky A A, Petruska M A, Hollingsworth J A, Htoon H, Bawendi M G and Klimov V I 2002 From amplified spontaneous emission to microring lasing using nanocrystal quantum dot solids *Appl. Phys. Lett.* **81** 1303
[34] Strauf S, Hennessy K, Rakher M T, Choi Y-S, Badolato A, Andreani L C, Hu E L, Petroff P M and Bouwmeester D 2006 Self-tuned quantum dot gain in photonic crystal lasers *Phys. Rev. Lett.* **96** 127404
[35] Banerjee A, Li R and Grebel H 2009 Surface plasmon lasers with quantum dots as gain media *Appl. Phys. Lett.* **95** 251106
[36] Johnson P B and Christy R W 1972 Optical constants of the noble metals *Phys. Rev.* B **6** 4370–9
[37] Song Y, Wang J, Li Q, Yan M and Qiu M 2010 Broadband coupler between silicon waveguide and hybrid plasmonic waveguide *Opt. Express* **18** 13173–9